We are IntechOpen, the world's leading publisher of Open Access books Built by scientists, for scientists

4,800
Open access books available

122,000
International authors and editors

135M
Downloads

Our authors are among the

154
Countries delivered to

TOP 1%
most cited scientists

12.2%
Contributors from top 500 universities

WEB OF SCIENCE™

Selection of our books indexed in the Book Citation Index in Web of Science™ Core Collection (BKCI)

Interested in publishing with us?
Contact book.department@intechopen.com

Numbers displayed above are based on latest data collected.
For more information visit www.intechopen.com

10

Mass Transfer Equation and Hydrodynamic Effects in Erosion-Corrosion

A. Yabuki
Hiroshima University
Japan

1. Introduction

Localized corrosion frequently occurs near the inlet of copper alloy heat exchanger tubes in seawater. Localized corrosion occurs when protective corrosion-product film that forms on the surface of the copper alloy is broken away by shear stress and turbulence causing the underlying metal surface to come into direct contact with the corrosive liquid. This phenomenon is known by several different terms: erosion-corrosion, flow-induced localized corrosion, flow-accelerated corrosion, or flow assisted corrosion (FAC), etc. (*Chexal et al.*, 1996; *Murakami et al.*, 2003). Damage by erosion-corrosion largely depends on hydrodynamic conditions such as the flow velocity of a liquid. Thus, this type of corrosion is characterized by the "breakaway velocity" at which the surface protective film is destroyed as the flow velocity increases (*Syrett*, 1976). To predict the extent of damage to copper alloys under a flowing solution, it is imperative to elucidate the relationships between damage to the materials and the hydrodynamic characteristics of the corrosive solution. Erosion-corrosion of copper alloys often proceeds via a diffusion-controlled process, and the mass-transfer equation for an oxidizing agent over the surface of a material is generally adopted. To apply the mass transfer equation to erosion-corrosion damage, mass transfer in both the concentration boundary layer and in the corrosion-product film on the material need to be considered, because the corrosion-product film that forms on the material confers a resistance to corrosion (*Mahato et al.*, 1980; *Matsumura et al.*, 1988). Flow velocity is generally used as the hydrodynamic parameter to predict erosion-corrosion damage, because it is quite simple. However, flow velocity is not sufficient to accurately predict damage, since erosion-corrosion frequently occurs in a turbulent region where the direction of flow changes, such as in a pipe bend, an elbow and or tee pipe fittings. Several papers have reported that the Sherwood number, a dimensionless number used in mass transfer operations, is useful as the mass transfer coefficient in the concentration boundary layer (*Sydberger et al.* 1982; *Poulson*, 1983, 1993, 1999; *Wharton*, 2004). Poulson reported that the Sherwood number in many flow conditions can be estimated through electrochemical measurements (*Poulson*, 1983). However, the Sherwood number also might inaccurately describe the condition of a corrosion-product film. Nešićet et al. conducted a numerical simulation of turbulent flow when a rust film was present, and found that fluctuations in turbulence affected both mass transfer through the boundary layer and the removal of the film (*Nešić et al.*, 1991). A numerical simulation of pipe flow has also been used to investigate erosion-corrosion (*Ferng et al.*, 2000; *Keating et al.*, 2001; *Postlethwaite et al.*, 1993; *Wharton et al.*, 2004).

This chapter on erosion-corrosion damage will discuss use of both the mass transfer equation as it relates to damage of materials and near-wall hydrodynamic effects to predict damage. Erosion-corrosion tests of copper alloys were conducted in a corrosive solution under various flow velocities using a jet-in-slit testing apparatus. A damage profile for each specimen was prepared using a surface roughness meter to evaluate local damage. The depth of the damage, calculated using the mass transfer equation, was related to the experimental data to confirm the applicability of the equation. Using the mass transfer coefficient of the corrosion-product films obtained from the mass transfer equation, the condition of the film and the breakaway properties were compared for each material. In addition, the near-wall hydrodynamic conditions at the material surface in the apparatus were measured using pressure gauges. The measured hydrodynamic conditions were applied to the equation used to predict the corrosion damage. The relationship between the near-wall hydrodynamic effects on the material surface and the corrosion of metallic materials under a flowing solution was investigated.

2. Erosion-corrosion damage

2.1 Experimental

The jet-in-slit testing apparatus used in the erosion-corrosion test is shown in Fig. 1. The testing apparatus consisted of a test solution tank, a pump, a flow meter and a test cell. Figure 2 shows a detailed schematic rendering of the test cell.

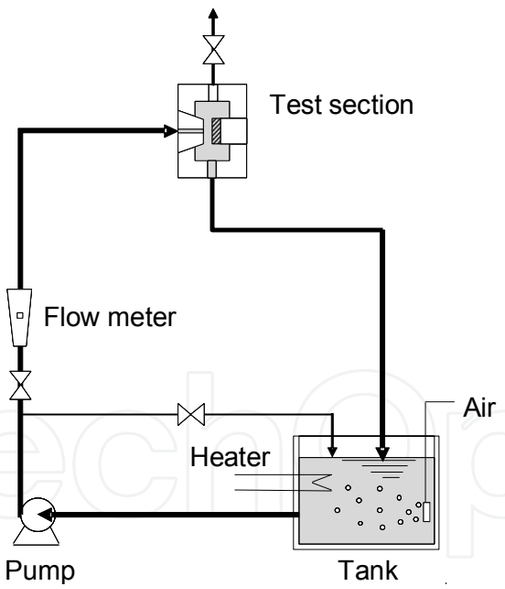

Fig. 1. Schematic diagram of a jet-in-slit testing apparatus.

In this apparatus, the test solution was allowed to flow from the nozzle into the slit between the specimen and the nozzle. The diameter of the specimen was 16 mm. The nozzle was made of a polymethyl-methacrylate resin with a bore diameter of 1.6 mm. The gap between the nozzle top and the specimen was 0.4 mm. As the solution was injected from the nozzle mouth into the slit, the solution filled the slit and flowed radially over the specimen surface. As the solution approached the periphery of the specimen, the cross-sectional area of the flow increased, and, consequently, the flow velocity decreased. The rapid reduction in flow

velocity created a shear stress and an intense turbulence in the flow, similar to what is expected downstream of orifice plates (*Matsumura et al.*, 1985). As a result, localized corrosion damage in the jet-in-slit test can be accounted for primarily by shear stress and the turbulence of the flow.

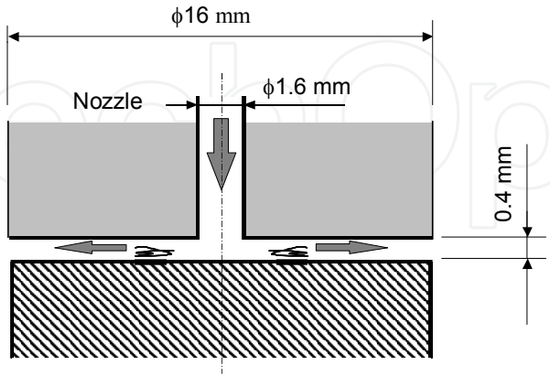

Fig. 2. Test section in the jet-in-slit corrosion-testing apparatus.

A 1 wt% $CuCl_2$ solution saturated with air was used as the test solution. Cu^{2+} was used as the oxidizing agent to accelerate the corrosion reaction. The temperature of the test solution was maintained at 40 ^{o}C. The flow velocities at the nozzle outlet were varied from 0.2 to 7.5 $m \cdot s^{-1}$. At a flow rate of 0.4 $L \cdot min^{-1}$, the fluid velocity at the nozzle outlet was 3.3 $m \cdot s^{-1}$ and the Reynold's number at that point was 8100. The test duration was 1 h.

The materials used in the investigation were pure copper (Cu) and three copper alloys, namely a beryllium copper alloy (BeCu) and two types of copper nickel alloys (70CuNi and 30CuNi). The chemical compositions of the test materials are shown in Table 1.

Symbol	Primary chemical composition / wt%
Cu	99.99Cu
70CuNi	30.2Ni-Cu
30CuNi	31.6Cu-Ni
BeCu	1.85Be-Cu

Table 1. Chemical composition of the copper alloys used in the tests.

Damage depth was determined by comparing the difference in the specimen surface profile before and after the test using a surface roughness meter and by determining the mass loss of the specimen. The damage depth rate was obtained by converting the maximum damage depth into $mm \cdot y^{-1}$.

2.2 Measurement of damage profiles

Cross-sectional profiles of the Cu and BeCu specimens after the test at a flow rate of 0.8 $L \cdot min^{-1}$ are shown in Fig. 3. The dotted line indicates the profile before the test as determined by the following: volume loss as calculated using measurement of the mass loss and the density of a specimen. The same position was used to measure the profile pre- and post-test, and then the difference between the two profiles was cylindrically integrated to obtain the volume loss. Then, the position was shifted vertically, and the procedure was repeated to determine if the

results coincided. Both the Cu and BeCu specimens were significantly damaged in the central region of the specimen (A) and in an area approximately 2 mm from the center of the specimen (B). The damage in region A was due to shear stress, while that in region B was due to turbulence, as described above (*Matsumura et al.*, 1985). The ratio of the damage in the central region A to that in region B was approximately two-thirds for the Cu specimen. On the other hand, the ratio for the BeCu specimen was approximately one-half. Thus, the damage to the BeCu specimen was much greater in the central region. This result indicates that the corrosion resistance of a corrosion-product film depends on the hydrodynamic conditions of a flowing solution. To evaluate in detail the role of the hydrodynamic effect in erosion-corrosion damage, the 1-mm radii of spots in the center regions of the damaged areas of the specimens and disturbed regions 2 to 3 mm from the center regions were chosen, and the maximal damage depths at both locations were measured under various velocities.

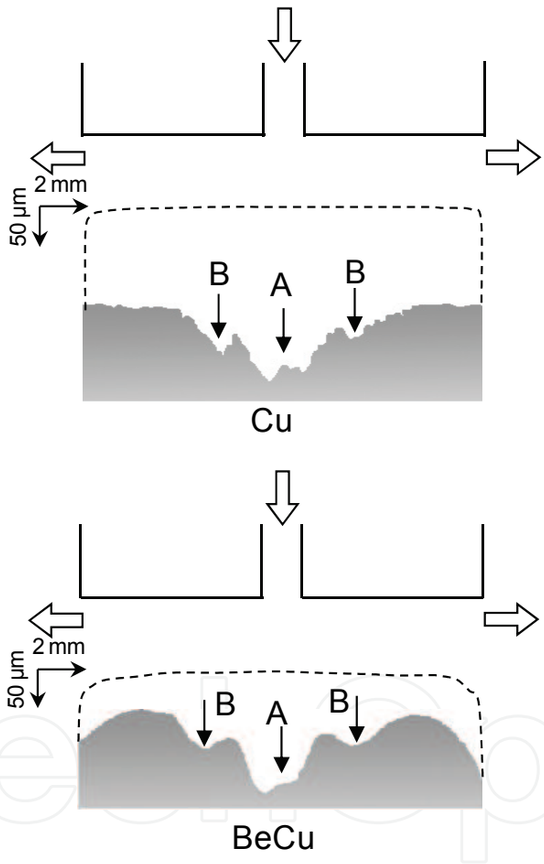

Fig. 3. Cross-sectional profile of a copper specimen (upper panel) and a BeCu specimen (lower panel) tested in a solution flowing at 0.8 L · min^{-1} for 1 h. The dotted line is the profile before the test. A and B are the central and disturbed regions.

3. Mass transfer equation in erosion-corrosion

3.1 Mass transfer equation

Various hydrodynamic parameters have been proposed to control the occurrence and extent of erosion-corrosion. The mass transfer coefficient is a parameter that relates the rate of a

diffusion-controlled reaction to the concentration driving force, and includes both diffusional and turbulent transport processes. Erosion-corrosion of copper alloys mainly proceeds under cathodic control because the rate-controlling step in corrosion is the transport of the oxidizing agent from the bulk of the fluid to the metal surface. When the surface of the copper alloy is exposed to a flowing fluid, a concentration boundary layer is formed in the bulk of the fluid outside of the corrosion-product film, as shown in Fig. 4.

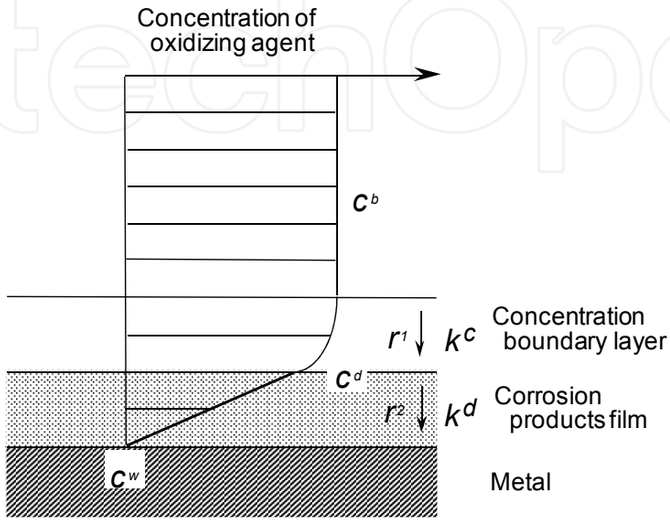

Fig. 4. Distribution of the oxidizing agent concentration in a solution flowing over a metal surface.

The diffusion rates of the oxidizing agent r_1 and r_2 in the concentration boundary layer and in the corrosion-product film, respectively, can be determined, as follows:

$$r_1 = k_c (c_b - c_d) \quad (1)$$

$$r_2 = k_d (c_d - c_w) \quad (2)$$

where c_b , c_d and c_w (mol · L^{-1}) are the oxidizing agent concentrations in the bulk of the flowing fluid, at the outside surface of the corrosion-product film, and at the metal surface, respectively. k_c and k_d (mm · y^{-1}) are the mass transfer coefficients in the concentration boundary layer and in the corrosion-product film, respectively.

The corrosion rate should be proportional to the diffusion rate of the oxidant. In the steady state, the mass transfer rates in the concentration boundary layer are equal to that in the corrosion-product film. Accordingly, the corrosion rate, R_c (mm · y^{-1}), can be given by the following reaction by using the conversion factor K (L · mol^{-1}):

$$R_c = K r_1 = K r_2 \quad (3)$$

The concentration of the oxidizing agent at the metal surface, c_w, may be zero (=0), since a very rapid electrochemical reaction is assumed. Equations (1)-(3) are combined to give:

$$R_c = K c_b / (1/k_c + 1/k_d) = c_b / (1/Kk_c + 1/Kk_d) \quad (4)$$

Equation (4) indicates that the corrosion rate is directly proportional to the concentration of the oxidizing agent, c_b, and inversely proportional to the combined resistance to mass

transfer, $1/Kk_c+1/Kk_d$. The concentration of the oxidizing agent, c_b , is 0.075 mol · L^{-1}, which corresponds to a $CuCl_2$ concentration of 1 wt%.

The issue of whether the mass transfer equation can be applied to the experimental results was examined. The problem is how to determine the mass transfer coefficients, k_c and k_d. According to the definition of the mass transfer coefficient, the coefficient in the concentration boundary layer, k_c, is inversely proportional to the thickness of the concentration boundary layer. It was previously determined that the thickness is dependent on the flow velocity and is inversely proportional to the velocity to the power of 0.5 for laminar flow and of 0.8 for turbulent flow (*Bird et al.*, 1960). Accordingly,

$$k_c \propto u^{0.5} \quad \text{(for laminar flow, Re<2300)} \tag{5}$$

$$k_c \propto u^{0.8} \quad \text{(for turbulent flow, Re>2300)} \tag{6}$$

It may be assumed that the mass transfer coefficient in the corrosion-product film, i.e., k_d, is also inversely proportional to the thickness of the corrosion-product film, but is initially independent of flow velocity, because the thickness of the corrosion-product film is nearly constant. After the increase in the corrosion rate, it is assumed that k_d depends on the flow velocity to the power, i.e., k_c. This is because the surface after the breakaway of the corrosion-product film consisted of a completely naked area, while at the same time the area was still covered with residual corrosion product (*Matsumura et al.*, 1985). Accordingly,

$$Kk_d = \alpha \text{ (constant, < breakaway velocity)} \tag{7}$$

$$Kk_d = \beta u^n \text{ (> breakaway velocity)} \tag{8}$$

where α, β and n are constants. Under these assumptions, Kk_c and Kk_d were determined and fitted the experimental data.

3.2 Damage depth rate and fitting by mass transfer equation

Figure 5 shows the relationship between the damage depth rate at the central and disturbed regions of a Cu specimen and the flow velocity. The solid curves in the figure were calculated using the mass transfer equation and fitted to the experimental data. Using the same procedure, the experimental data and the fitted lines for BeCu, 70CuNi and 30CuNi are shown in Figs. 6, 7 and 8, respectively. The coefficient in the concentration boundary layer, Kk_c, was determined and used to fit the experimental data. The constants α, β and n in equation (7) and (8), which are related to the mass transfer coefficient in a corrosion-product film, are listed in Table 2. These parameters are discussed below.

The damage depth for the Cu specimen increased slightly with increasing flow velocity at lower velocities (Fig. 5). The damage depth increased rapidly at a certain velocity, namely the breakaway velocity (*Syrett*, 1976). The breakaway velocity at the central region was 2 m · s^{-1} and at the disturbed regions it was 0.8 m · s^{-1}. The damage depth at a velocity less than the breakaway velocity for the central and disturbed regions fit the same curve. The damage depth doubled at the breakaway velocity in both regions, and further increased at higher flow velocities. This result indicates that the corrosion-product film formed on the Cu was easily broken away by the turbulence that occurred in the disturbed regions, and was not due to shear stress. It was confirmed that the damage depth, determined by the mass transfer equation, was well fitted to experimental damage depth for Cu, although the damage varied at different regions of the specimen.

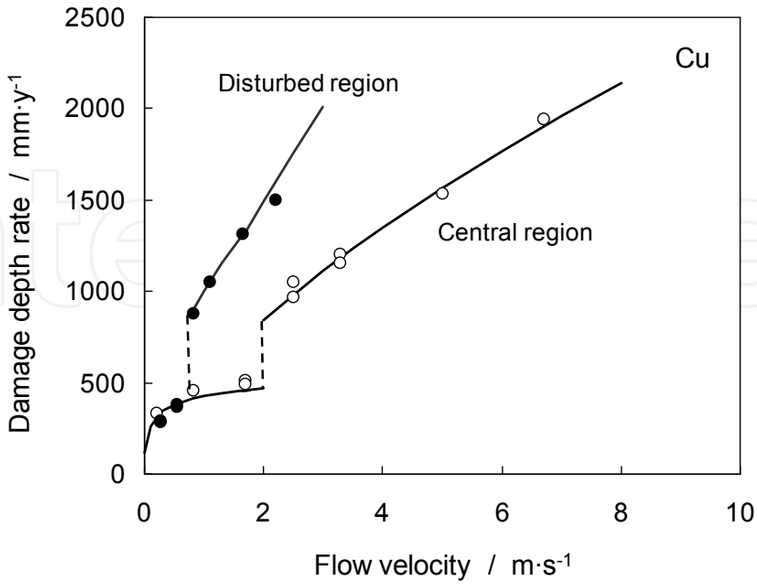

Fig. 5. Relationship between flow velocity and damage depth rate at the central and disturbed regions of a pure copper (Cu) specimen tested in a jet-in-slit testing apparatus. The curves were calculated using the mass transfer equation as fitted to the experimental data.

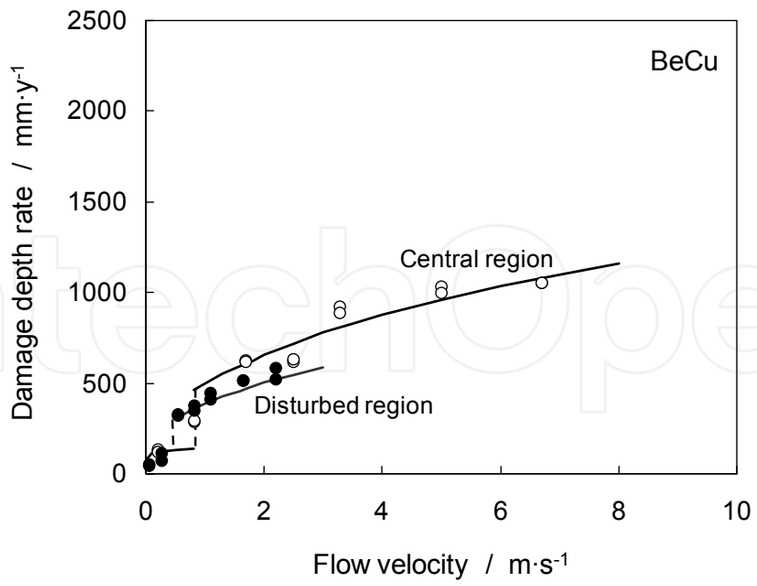

Fig. 6. Relationship between the flow velocity and damage depth rate in the central and disturbed regions of a beryllium copper alloy (BeCu) specimen tested in a jet-in-slit testing apparatus. Curves were calculated by using the mass transfer equation as fitted to the experimental data.

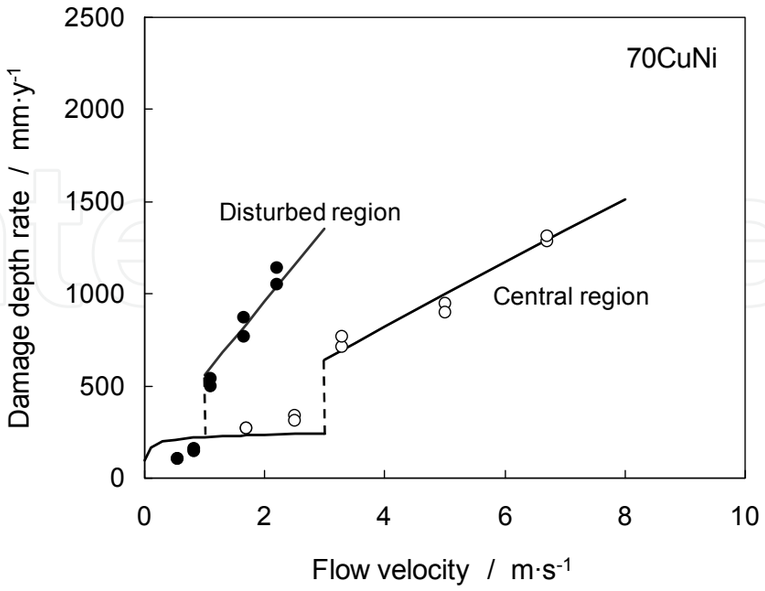

Fig. 7. Relationship between the flow velocity and damage depth rate in the central and disturbed regions of a copper nickel alloy (70CuNi) specimen tested in a jet-in-slit testing apparatus. Curves were calculated using the mass transfer equation as fitted to the experimental data.

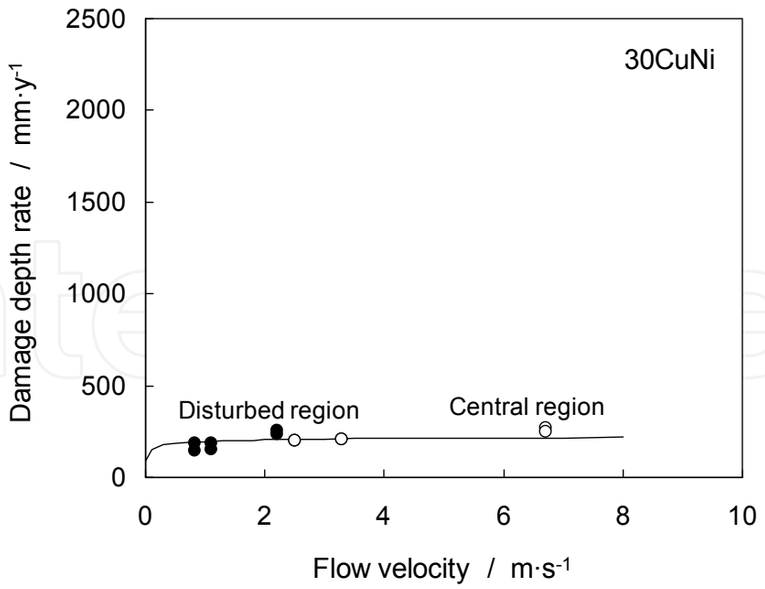

Fig. 8. Relationship between the flow velocity and damage depth rate in the central and disturbed regions of a copper nickel alloy (30CuNi) specimen tested in a jet-in-slit testing apparatus. Curves were calculated using mass transfer equation as fitted to the experimental data.

Symbol	Region	V_b / m · s^{-1}	α	β	n
Cu	Central	2	8000	12000	0.6
	Disturbed	0.8	↑	40000	↑
BeCu	Central	0.8	2000	10000	0.3
	Disturbed	0.5	↑	7000	↑
70CuNi	Central	3	3500	4000	0.9
	Disturbed	1	↑	12000	↑
30CuNi	Central	-	3000	-	-
	Disturbed	-	↑	-	-

Table 2. Constants for the mass transfer equation determined as fitted to the damage depth rate of each copper alloy.

The damage depth rate for the BeCu specimen increased with increasing flow velocity, but was relatively low, compared to the rate for the Cu specimen (Fig. 6). The breakaway velocity at the central region was 0.8 m · s^{-1}, while that in the disturbed region was 0.5 m · s^{-1}. Moreover, the breakaway velocity was lower than that for the Cu specimen. The damage depth rate was very low at velocities less than the breakaway velocity, compared to the rate for the Cu specimen. At velocities greater than the breakaway velocity, the damage depth rate increased slightly with increasing flow velocity. However, the behavior of the damage depth rate was similar in both the central and disturbed regions. The corrosion behavior of the BeCu specimen was different from that of the Cu specimen. The damage depth rate, calculated from the mass transfer equation, could also be fitted to the experimental data for the BeCu sample.

For the 70CuNi alloy, the breakaway velocity in the central regions was 3 m · s^{-1}, while that in the disturbed region was 1 m · s^{-1} (Fig. 7). The damage depth rate at the breakaway velocity was increased three-fold, and also increased with an additional increase in the flow velocity. Although the damage was low compared to the damage to the Cu specimen, the corrosion behavior was similar to that of the Cu specimen. This result was attributed to the formation of a good quality anti-corrosion film due to the addition of nickel. The damage depth rate at a velocity lower than the breakaway velocity was linear, but the curve calculated from the mass transfer equation did not coincide with the experimental damage rate. This result was apparently caused by a slight breakaway of the film, although the damage was not fatal. The damage depth rate at a velocity higher than the breakaway velocity simulated the experimental rate.

The damage depth rate for the 30CuNi alloy was constant at both the central and disturbed regions under all velocities (Fig. 8). This result shows that 30CuNi is an excellent film for protecting against erosion-corrosion, even when the flow velocity is high. The damage depth rate calculated from the mass transfer equation was well-fitted to the experimental results.

The damage depth rate at the central region differed from that at the disturbed region, and was dependent on hydrodynamic conditions. However, it was confirmed that the mass transfer equation and the assumptions concerning the corrosion-product film as described by equations (7) and (8) can be applied to erosion-corrosion damage.

3.3 Characterization of film

The relationships between the flow velocity and the mass transfer coefficient in a corrosion-product film (Kk_d) in the central regions of each specimen are shown in Fig. 9. The mass

transfer coefficient in the concentration boundary layer, Kk_c, is shown by the dotted line in the figure. The dashed lines in the Kk_d curves show the breakaway velocities for each material.

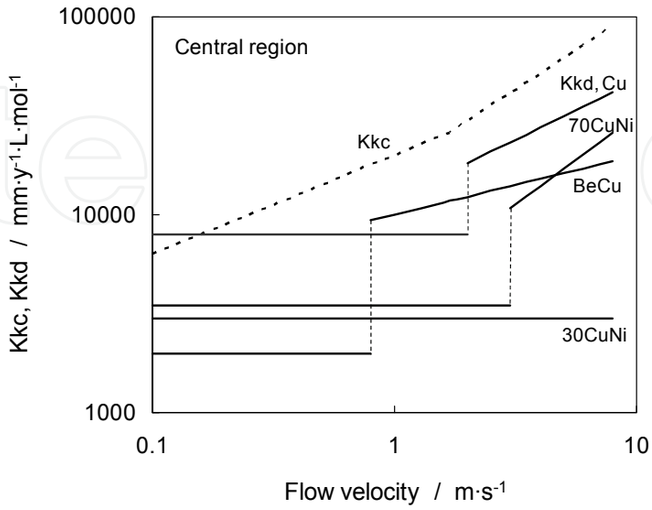

Fig. 9. Values of Kk_c and Kk_d determined by fitting to the damage depth rate in the central region of a specimen.

The mass transfer coefficient in the corrosion-product film, Kk_d, of Cu was very similar to the mass transfer coefficient of the concentration boundary layer, Kk_c, at a velocity less than the breakaway velocity. Therefore, the damage rate for Cu depends on the concentration boundary layer at lower velocities. However, the damage rate of the other copper alloys is determined by the condition of the corrosion-product film, because the Kkd of the other copper alloys was very low compared with Kk_c. This is equivalent to α, as shown in Table 2, and the corrosion resistance of the films that formed on BeCu, 70CuNi and 30CuNi was enhanced more than two-fold compared to the film that formed on pure Cu. At a velocity higher than the breakaway velocity, the Kk_d for the copper alloys was always lower than Kk_c. Consequently, the damage rate was mostly dependent on the mass transfer rate in the corrosion-product film. In other words, the damage rate is determined only by the corrosion-product film. At velocities higher than the breakaway velocity, the slope of Kk_d , listed in Table 2 as a power of n, was quite different for each material. The constant n appears to be the breakaway property of the film that formed on each material. The constant n for Cu was 0.6, which was similar to the change in the thickness of the concentration boundary layer and the same as Kk_c. The film that formed on BeCu was resistant to breakaway, since the constant for BeCu was as low as 0.3. The breakaway property of the film that formed on 70CuNi was nearly proportional to the flow velocity, since the constant, n, was 0.9. Thus, these results confirm that the breakaway property of each material was different at the central region, where the shear stress was dominant.

The relationships between the flow velocity and the mass transfer coefficient in the corrosion-product film (Kk_d) at the disturbed regions of each specimen are shown in Fig. 10. At velocities less than the breakaway velocity, the behavior observed in the disturbed regions was the same as that observed in the central region. At velocities higher than the breakaway velocity, the Kk_d for Cu exceeded the value of Kk_c. This result indicates that

mass transfer in the concentration boundary layer was dominant, although small amounts of the corrosion-product film might remain on the specimen surface. The damage to the 70CuNi alloy affected both mass transfer coefficients, since the Kk_d for 70CuNi was comparable to Kk_c. The Kk_d for BeCu was so low that mass transfer in the corrosion-product film was dominant, as in the central region. The power, n, of the exponential equation for Kk_d at velocities higher than the breakaway velocity was different for each material, however, it was the same as that in the central region. Thus, although the extent of breakaway of the films that formed on each material was dependent on the hydrodynamic conditions, the increasing ratio for breakaway of the film with flow velocity was not dependent on hydrodynamics, but on the type of material.

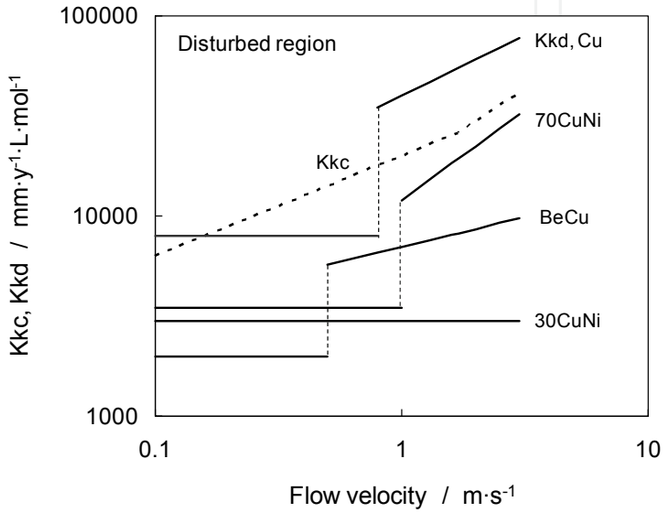

Fig. 10. Values of Kk_c and Kk_d determined by fitting to the damage depth rate in the disturbed region of the specimens.

Consequently, to predict erosion-corrosion damage for a copper-based material, the mass transfer equation can be used as a fundamental equation. However, the flow velocity does not adequately express various hydrodynamic conditions such as turbulence or shear stress. The Sherwood number seems to be more suitable than the flow velocity. Of course, the mass transfer coefficient in the concentration boundary layer can be predicted. However, prediction of the mass transfer coefficient in a corrosion-product film appears difficult, because the Sherwood number is almost propotional to the flow velocity at a Reynold's number of less than 10,000 in an impinging jet testing apparatus similar to the apparatus used in the present study (*Sydberger et al.*, 1982). An alternative parameter to describe hydrodynamic conditions rather than the flow velocity or the Sherwood number is desirable for prediction of the breakaway properties of a corrosion-product film. The corrosion-product film that formed on pure Cu tested at a lower flow velocity consisted of numerous particles, which were approximately 5 μm in diameter. Thus, breakaway of the corrosion-product film was equivalent to particle removal due to the hydrodynamic action of the flowing solution. Concerning the removal of the particles, it is important to investigate the relationships between particle morphology and adhesive force. Thus, selection of a hydrodynamic parameter related to erosion-corrosion was the most important issue initially. The mass transfer coefficient can be determined by electrochemical measurements,

but it was thought that determination of the force acting on the surface of the material, for instance, a pressure measurement, was also useful. It is reasonable to use the mass transfer equation as a basic equation. A more complex equation should be developed for prediction of erosion-corrosion damage in an actual machine, along with a numerical simulation (*Ferng et al.*, 2000; *Keating et al.*, 2001; *Postlethwaite et al.*, 1993).

4. Hydrodynamic effects

4.1 Measurement of near-wall hydrodynamic conditions

The near-wall hydrodynamic conditions of each specimen were measured in the jet-in-slit corrosion testing apparatus using two pressure gauges and a wire. The set-up for the system is shown in Fig. 11. The fluid in the tank flows to a nozzle through a flow meter with a pump, and then returns to the tank. Three types of nozzles were prepared. One was the same size as the nozzle of the corrosion testing apparatus, and the others were 2-fold and 5-fold scale-ups. The fluid velocity at the nozzle equaled that of the corrosion testing apparatus. Two holes, each 0.3 mm in diameter, were bored into the surface of the measurement plate, and a wire 0.05 mm in diameter was set between the holes, as shown in Fig. 12.

Pressure gauges (PGM-02KG, Kyowa Electronic Instruments Co., Ltd.) were connected to the holes. The signal from each pressure gauge was input to a personal computer through a sensor interface (PCD-300, Kyowa Electronic Instruments Co., Ltd.). The horizontal velocity V_x ($m \cdot s^{-1}$) and the vertical velocity V_y ($m \cdot s^{-1}$) were calculated by the pressure differential $\Delta P=P_1-P_2$ (Pa) and the wall pressure upstream of the wire, P_1 (Pa), respectively. The measured pressure was converted into velocity using equations (9) and (10), which are given by Bernoulli's law,

$$V_x = (2\Delta P/\rho)^{0.5} \tag{9}$$

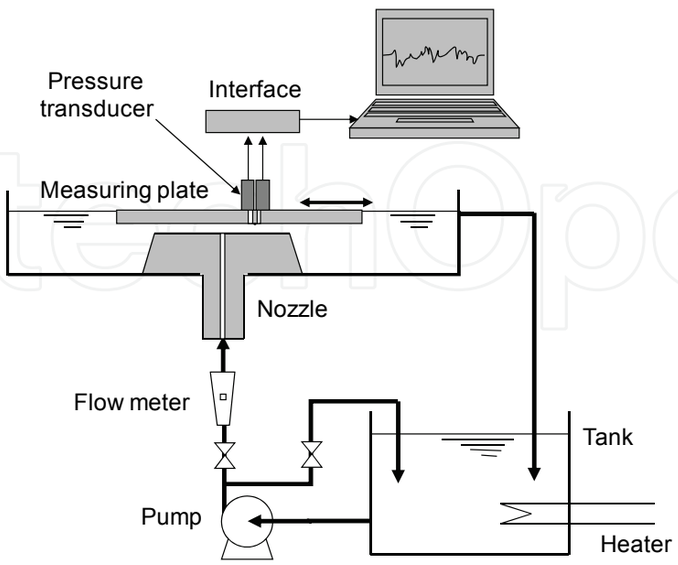

Fig. 11. Set-up for the system to measure the near-wall hydrodynamic conditions of a specimen in the jet-in-slit corrosion testing apparatus.

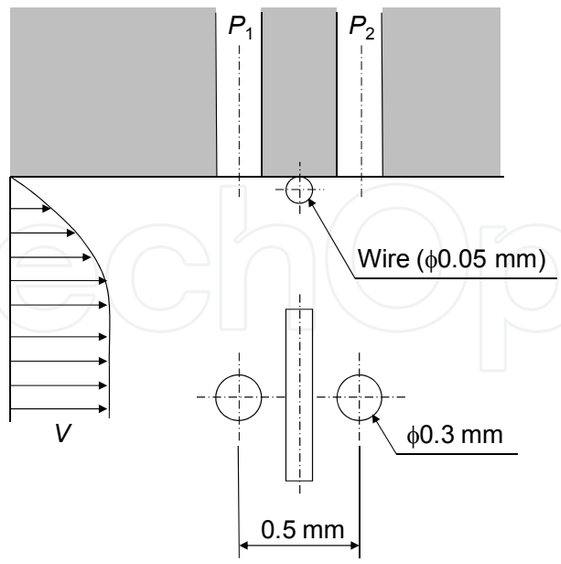

Fig. 12. Dimensions of the two holes connected to the pressure gauges and the wire set on the measuring plate for determination of near-wall hydrodynamic conditions.

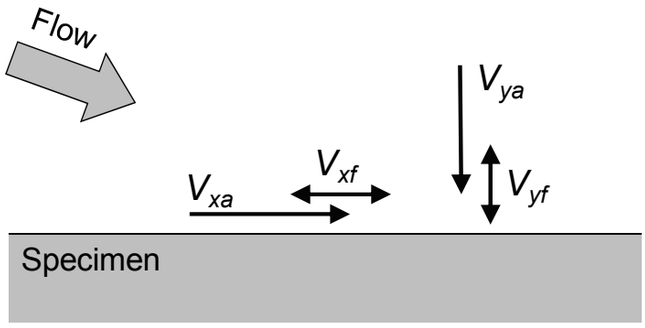

Fig. 13. The near-wall average velocity and the fluctuation in the horizontal (x) and vertical (y) directions relative to the specimen surface, V_{xa}, V_{xf}, V_{ya} and V_{yf}.

$$V_y=(2P_1/\rho)^{0.5} \tag{10}$$

where ρ (kg· m^{-3}) is the density of the solution. The measuring plate was moved from the center of the nozzle mouth to the periphery to measure each point on the specimen surface.

Only the distributions in the right-half of the apparatus were measured, since the left-half distributions should be nearly identical to those of the right side. The sampling time was 10 s and the sampling frequency was 2 kHz. The average velocities and the fluctuations in the horizontal (x) and vertical (y) directions relative to the specimen surface, V_{xa}, V_{xf}, V_{ya} and V_{yf} (as shown in Fig. 13), were calculated from the time dependence of the horizontal velocity V_x and the vertical velocity V_y, respectively. V_{xa} and V_{ya} are equal to the wall shear stress and the hydrodynamic energy density, respectively (*S. Nešić et al., 1991; Bozzini et al., 2003*).

4.2 Near-wall hydrodynamic conditions

Near-wall hydrodynamic conditions in the jet-in-slit apparatus were measured using three types of nozzles. The distribution of the hydrodynamic conditions, which were measured using the same nozzle as was used in the corrosion testing apparatus, did not appear smooth, because the holes for the pressure gauge and wire were too large. However, the distributions of the hydrodynamic conditions that were measured using the nozzles that were scaled-up 2- and 5-fold, were very smooth and nearly identical. The measurement points were easily adjusted using the nozzle that was scaled-up 5-fold. Therefore, that nozzle was used to measure the near-wall hydrodynamic conditions. To compare the hydrodynamic conditions with the corrosion damage, the region in which the hydrodynamic conditions were measured corresponds to the nozzle in the corrosion testing apparatus. Thus, the value of that region was divided by 5.

The time-dependence of the pressure differential was located 1.5 mm from the center of the specimen (ΔP), and the wall pressure was at the center of the specimen, P_1, and both are shown in Fig. 14. Fluctuations in ΔP and P_1 were detected, and the frequencies were approximately 200 Hz and 130 Hz, respectively. The frequencies were not the same in both areas, so the fluctuations must have been due to the vibration of the fluid rather than to the pulsation of the pump.

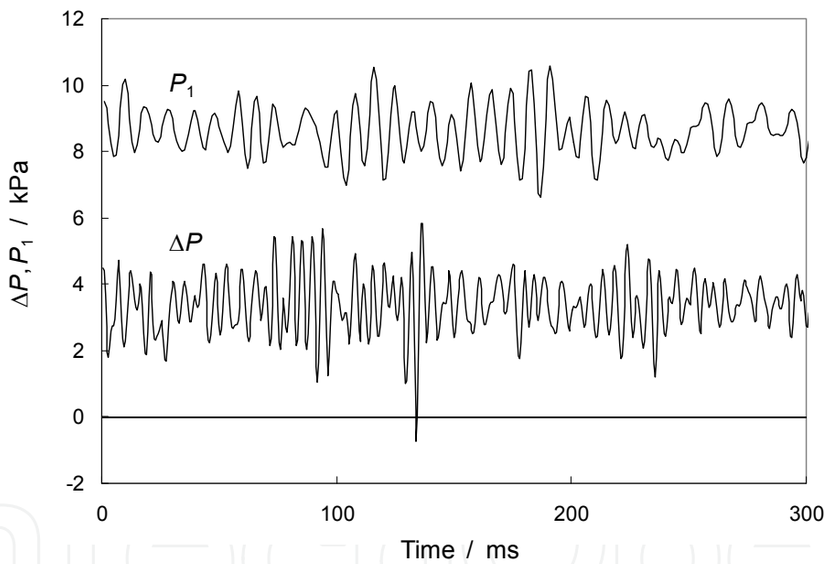

Fig. 14. Time-dependence of the pressure differential located 1.5 mm from the center of the specimen (ΔP) and the wall pressure at the center of the specimen (P_1).

ΔP and P_1, which were measured by pressure gauges were converted into horizontal velocity (V_x) and vertical velocity (V_y) using equations (9) and (10), respectively. Furthermore, the horizontal velocity V_x was calculated from the average velocity V_{xa} and the fluctuation V_{xf}. V_{xf} was 3 times the standard deviation of the velocity. The vertical velocity and the horizontal velocity were also used to calculate V_{ya} and V_{yf}. The distributions of the velocities and the fluctuations in the horizontal and vertical directions were obtained by moving the measuring plate.

Fig. 15 shows the distributions of the near-wall hydrodynamic conditions, V_{xa}, V_{xf}, V_{ya}, and V_{yf}, of the specimens. Only the distributions in the right-half of the apparatus are shown in

the figure. The average vertical velocity, V_{ya}, was highest at the center of the specimen, since the solution was injected vertically and toward the specimen. V_{ya} showed a negative pressure in the area outside of 5 mm, which was due to boundary-layer separation in the area. The average horizontal velocity V_{xa} was highest 5 mm from the center of the specimen, which corresponded to the edge of the nozzle mouth, because the flow direction changed at this location. The fluctuations in the vertical and horizontal velocities V_{ya} and V_{yf} were highest in the area 10 mm from the center. As a result, the hydrodynamic parameters had different distributions, and the region showing the maximum differed among these parameters. Thus, we successfully measured the various hydrodynamic parameters in the jet-in-slit corrosion testing apparatus.

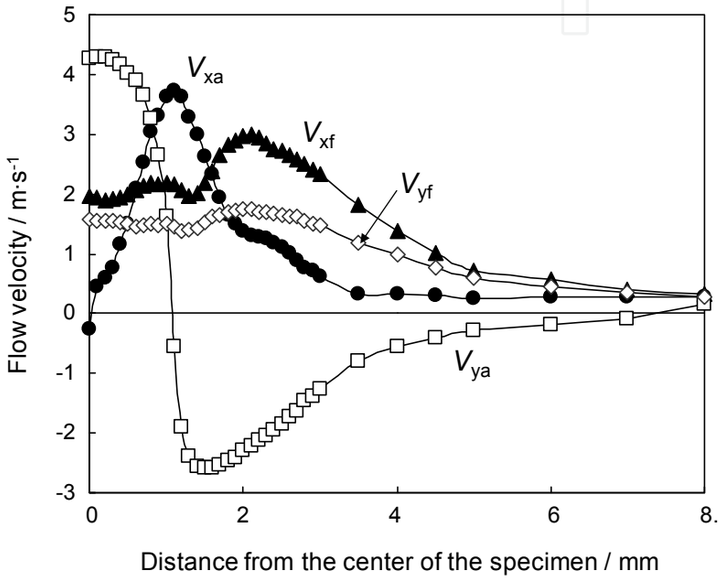

Fig. 15. The distributions of the near-wall hydrodynamic conditions, V_{xa}, V_{xf}, V_{ya} and V_{yf}, of the specimens. Only the distributions in the right-half of the apparatus are shown in the figure.

To relate the hydrodynamic conditions to the corrosion damage, V_{xa}, V_{xf} and V_{ya} were selected as follows. Only positive pressure was used for V_{ya}, because negative pressure in the area outside the region 5 mm from the center was caused by boundary-layer separation and was related to the fluctuations V_{xf} and V_{xf}. The vertical velocity fluctuation V_{yf} was similar to the horizontal velocity fluctuation V_{xf}, so only V_{xf} was used to predict the corrosion damage.

4.3 Prediction of damage using hydrodynamic effects and mass transfer equation

The jet-in-slit testing apparatus shown in section 2.1 was used for the corrosion tests performed under a flowing solution. Brass (58.3Cu-38.2Zn-3.10Pb-0.17Fe-0.23Sn) and 70CuNi (30.2Ni-Cu) were used as model materials for the corrosion tests. A 3% NaCl solution and a 1 wt% $CuCl_2$ solution saturated with air were used as the corrosive test solutions. The concentration of oxygen dissolved in the solutions was approximately 6.45 ppm. Cu^{2+} in the 1 wt% $CuCl_2$ solution acted as the oxidizing agent to accelerate the corrosion reaction. The test duration was 24 h in the 3% NaCl solution and 1 h in the 1 wt% $CuCl_2$ solution.

Cross-sectional profiles of the brass and 70CuNi specimens after flow-induced localized corrosion tests at a flow rate of 0.4 L · min^{-1} are shown in Fig. 16. The thin line indicates the profile before the test, which was determined as volume loss calculated from mass loss and the density of a specimen coinciding to the volume loss calculated from the surface profile before and after the test, as explained in section 2.2.

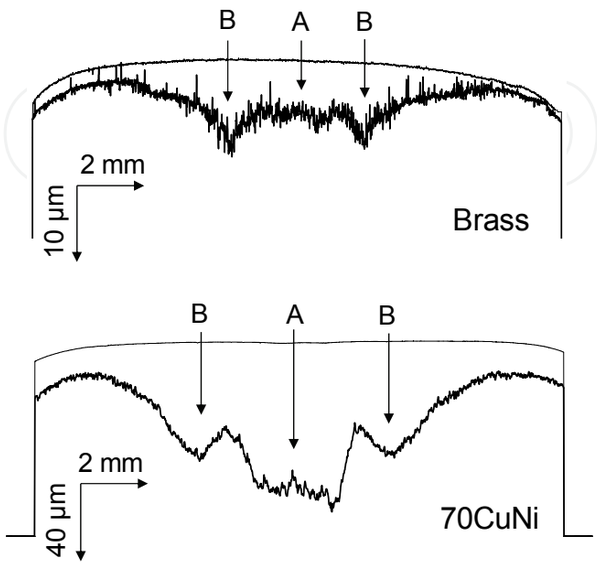

Fig. 16. Cross-sectional profiles of the brass (upper) and 70CuNi (lower) specimens after flow-induced corrosion tests at a flow rate of 0.4 L min^{-1}. The thin line is the profile before the test.

Brass was significantly damaged in the central region of the specimen (region A) and in the area approximately 2 mm from the center of the specimen (region B). The damage to the periphery was relatively low. This result was obviously due to the hydrodynamic effects of the corrosive solution. Similar to the brass specimen, the 70CuNi sample was significantly damaged in the central area (regions A and B), compared with the damage to the periphery. The damage in region B was deeper than that in region A for brass, but the damage in region B was less than that in region A for 70CuNi. The result is likely due to differences in the corrosion-product films that formed on the surface of each specimen under a flowing solution, because the hydrodynamic conditions near the surface were very similar for the two materials. The corrosion rate for both materials differed with the oxidizing agent concentration. The flow-induced localized corrosion of copper alloys proceeded through both the initiation step, which occurred following the mechanical destruction of the corrosion-product film, and the propagation step, which occurred following the repeated formation and breakaway of the products due to the local hydrodynamic effect (*S. Nešić et al., 1991; Bozzini et al., 2003*). Since wet-polished specimens were tested in the present study, most of the damage to the copper alloys occurred during the propagation step, which was equal to the steady state. The porous corrosion-product film was detected by direct observation of the specimen surface after the corrosion test.

The corrosion damage to the copper alloy in a 1 wt% $CuCl_2$ solution was much greater than the damage that resulted from the 3% NaCl solution, as shown in Fig. 16. This result indicated that the corrosion damage was mainly caused by the cathodic reaction. Thus, the

flow-induced localized corrosion of copper alloys mainly proceeds under cathodic control, so that the rate-controlling step in corrosion is the transport of the oxidizing agent from the bulk of the fluid to the metal surface. The corrosion rate should be proportional to the diffusion rate of the oxidant. In the steady state, the corrosion rate, R_c ($m \cdot s^{-1}$), can be given by equation (4). Accordingly, the local damage d (μm) can be estimated using the testing time t (h), as follows:

$$d = 3.6\times10^{9}\, K c_b\, t \,/\, (1/k_c + 1/k_d) \tag{11}$$

Assuming that the corrosion-product film that formed on the copper alloys was either thicker than the concentration boundary layer or thinner but more dense, it had a structure that resisted diffusion of the oxidizing agent. Therefore, the diffusion of the oxidizing agent in the corrosion-product film was relatively low for the rate-controlling step, namely $k_c >> k_d$. Thus equation (11) gives

$$d = 3.6\times10^{9}\, K k_d\, c_b\, t \tag{12}$$

The corrosion-product film that formed on the surface was in a steady state, and its thickness and structure were determined by repeated formation and breakaway due to the hydrodynamic effects. In this process, the condition of the film is determined by the mechanical force acting on the film. When the velocity was high, the force acting on the film was large, resulting in thinning of the film, so that the mass transfer coefficient in the corrosion-product film became larger. Hence, the mass transfer coefficient in the corrosion-product film k_d ($m \cdot s^{-1}$) was assumed to be proportional to the velocities at the near-wall, as follows:

$$k_d = \gamma_{xa} V_{xa} + \gamma_{xf} V_{xf} + \gamma_{ya} V_{ya} \tag{13}$$

where each γ is a material-specific constant that corresponds to the contributing ratio for each hydrodynamic condition.

The damage depth profile for the copper alloys was calculated using equations (12) and (13) as fitted to the experimental damage profile using a trial-and-error method. The calculated and experimental profiles for brass and 70CuNi are shown in Figs. 17 and 18. The figures show only the right-half of the damage profile for each specimen. The data used for brass that was tested in a 3% NaCl solution were as follows: $K = 3.6\times10^{-6}$ $m^3 \cdot mol^{-1}$ (= $63.5/2/8.9\times10^{6}$, where 63.5 $g \cdot mol^{-1}$ is the molecular weight of copper, 2 is the number of ion-exchanges in anodic and cathodic reactions, and 8.9×10^{6} $g \cdot m^{-3}$ is the density of copper), c_b = 0.20 $mol \cdot m^{-3}$, which corresponds to dissolved oxygen of 6.45 ppm, t=24 h, and the γ values obtained by fitting to the measured data were: $\gamma_{xa} = 2.3\times10^{-7}$, $\gamma_{xf} = 4.6\times10^{-5}$ and $\gamma_{ya} = 1.2\times0^{-6}$, respectively.

The data used for 70CuNi that was tested in a 1 wt% $CuCl_2$ solution were as follows: K = 7.1 x 10^{-6} $m^3 \cdot mol^{-1}$ (=$63.5/1/8.9\times10^{6}$, where 63.5 $g \cdot mol^{-1}$ is the molecular weight of copper, 1 is the number of ion-exchanges in anodic and cathodic reactions, and 8.9×10^{6} $g \cdot m^{-3}$ is the density of 70CuNi). c_b = 74 $mol \cdot m^{-3}$, which corresponds to the Cu^+ concentration of the 1 wt% $CuCl_2$ solution, t = 1 h, and the γ values obtained for each material from fitting to the measured data were: $\gamma_{xa} = 3.8\times10^{-6}$, $\gamma_{xf} = 8.8\times10^{-6}$, $\gamma_{ya} = 3.5\times10^{-6}$, respectively. The calculated profiles were consistent with both the experimental data and the areas of maximal damage for both copper alloys—2 mm for brass and 1 mm for 70CuNi. Comparing the contributing ratio (γ) to each hydrodynamic condition, the fluctuation in horizontal velocity, γ_{xf}, was

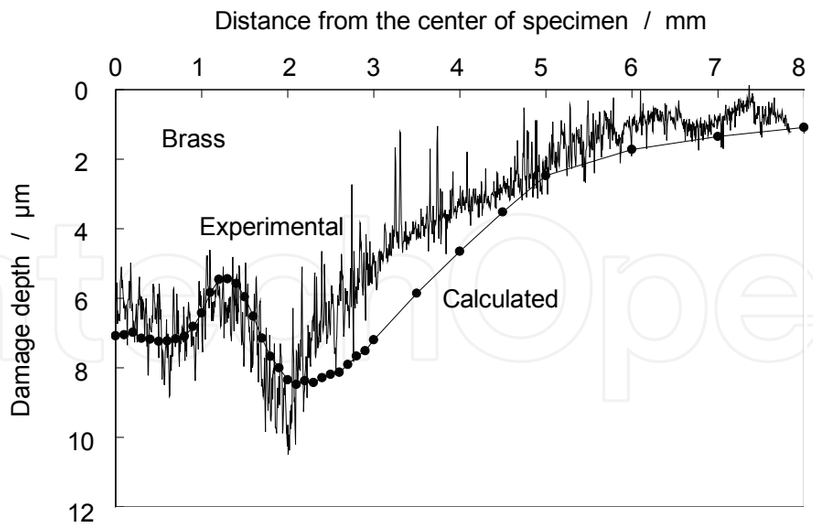

Fig. 17. The experimental and calculated damage depth profiles for brass tested in the 3% NaCl solution for 24 h. The figures show only the right half of the specimen.

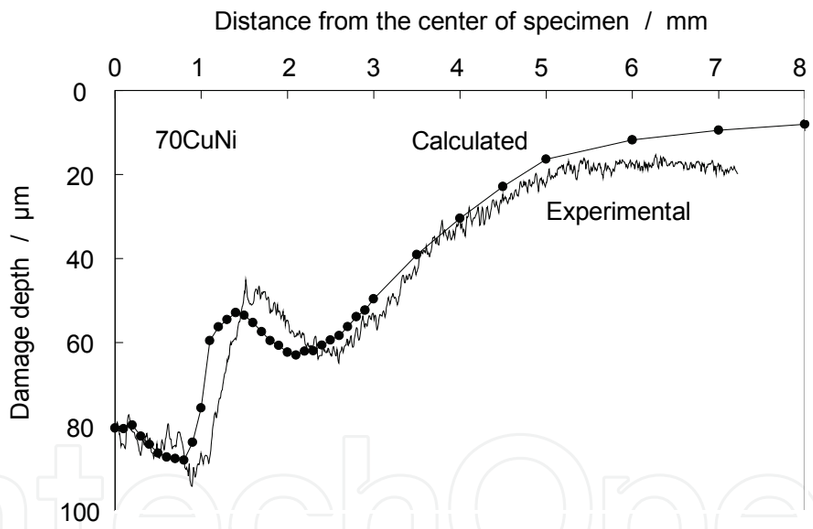

Fig. 18. The experimental and calculated damage depth profiles for 70CuNi tested in the 1 wt% $CuCl_2$ solution for 1 h. The figures show only the right half of the specimen.

dominant in the corrosion damage of brass. On the other hand, average vertical velocity, γ_{xa}, also affected the corrosion damage of 70CuNi, in addition to the fluctuation of horizontal velocity, γ_{xf}. Thus, the hydrodynamic effect on the corrosion damage of copper alloys was not attributed to a single parameter, such as flow velocity or Sherwood number, but instead was related to multiple effects from both horizontal and vertical force and fluctuation. The material-specific constant γ in equation (13) is related to the mechanical properties of the corrosion-product films that formed on the surface of copper alloys. Consequently, these properties are particularly important for the prediction of corrosion damage under a flowing solution.

7. Conclusion

Erosion-corrosion tests were carried out using a jet-in-slit testing apparatus, and the following results were obtained. The damage depth rate of Cu, BeCu and 70CuNi increased with increasing flow velocity, and the breakaway velocity was clearly evident. The films that formed on Cu and 70CuNi were significantly damaged by turbulence, such that the hydrodynamic conditions of the flowing solution affected the breakaway property of the corrosion-product film. Damage depth rate, calculated by the mass transfer equation, which involved mass transfer in the concentration diffusion layer and in the corrosion-product film, could to be fitted to the experimental damage rate. Thus, we confirmed that the mass transfer equation can be applied to erosion-corrosion damage to copper and copper alloys. The film condition remained nearly constant at a velocity lower than the breakaway velocity, and the films that formed on BeCu, 70CuNi and 30CuNi were enhanced more than two-fold compared with the film that formed on pure Cu, as evidenced by the analysis of the mass transfer coefficient in the corrosion-product film. The corrosion-product film was exponentially broken away at velocities greater than the breakaway velocity. The breakaway property of the corrosion-product film differed among the materials, since the power of the exponential equation was different for each material.

The relationship between the near-wall hydrodynamic effects on the material surface and the corrosion damage of material under a flowing solution was investigated. The near-wall hydrodynamic conditions on the surface of the test specimens were measured using pressure gauges, and both the distribution of the near-wall velocity and the velocity fluctuations were determined. Three types of hydrodynamic conditions were applied as parameters that are related to the mass transfer coefficient in a corrosion-product film in the equation used to predict corrosion damage. The damage profiles calculated from the equation could be fitted to that obtained from the corrosion test using the three hydrodynamic parameters. The determined material-specific constant agreed with the mechanical resistance of the corrosion-product film to the hydrodynamic effects in a corrosive liquid. Consequently, the mechanical properties of the corrosion-product films that formed on the surface of the copper alloys are particularly important for the prediction of corrosion damage under a flowing solution.

8. References

Bird R.B.; Stewart W.E. & Lightfoot E.N. (1960). *Transport phenomena*, John Wiliey & Sons, INC., pp. 647, ISBN 0-471-07392-X, New York.

Bozzini B.; Ricotti M.E.; Boniardi M. & Mele C. (2003). Evaluation of erosion–corrosion in multiphase flow via CFD and experimental analysis, *Wear*, Vol.255, No.1-6, 237-245, ISSN 0043-1648.

Chexal B.; Horowitz J.; Jones R.; Dooley B.; Wood C.; Bouchacourt M.; Remy F.; Nordmann F. & Paul P.St. (1996). *Flow-Accelerated Corrosion in Power Plants*, EPRI Distribution Center, ISBN TR-106611, Pleasant Hill, CA.

Ferng Y.M.; Ma Y.P. & Chung N.M. (2000). Application of local flow models in predicting distributions of erosion-corrosion locations, *Corrosion*, Vol.56, No.2, 116-126, ISSN 0010-9312.

Keating A. & Nešić S. (2001). Numerical prediction of erosion-corrosion in bends, *Corrosion*, Vol.57, No.7, 621-633, ISSN 0010-9312.

Mahato B.K.; Cha C.Y. & Shemilt L.W. (1980). Unsteady state mass transfer coefficients controlling steel pipe corrosion under isothermal flow conditions, *Corrosion Science*, Vol.20, No.3, 421-441, ISSN 0010-938X.

Matsumura M.; Oka Y.; Okumoto S. & Furuya H. (1985). *Laboratory Corrosion Tests and Standards STP 866*, ASTM, pp.358-372, ISBN 0-8031-0443-X, Philadelphia.

Matsumura M.; Noishiki K. & Sakamoto A. (1988). Jet-in-slit test for reproducing flow-induced localized corrosion on copper alloys, *Corrosion*, Vol.54, 79-88, ISSN 0010-9312.

Murakami, M.; Sugita K.; Yabuki A & Matsumura M. (2003). Mechanism of so-called erosion-corrosion and flow velocity difference corrosion of pure copper, *Corrosion Engineering (Zairyo-to-Kankyo)*, Vol.52, No. 3, 155-159, ISSN 0917-0480.

Nešić S. & Postlethwaite J. (1991). Hydrodynamics of disturbed flow and erosion-corrosion. Part I-Single-phase flow study, The Canadian Journal of Chemical Engineering, Vol.69, No. 3, 698-703, ISSN 00084034.

Postlethwaite J.; Nešić S.; Adamopoulos G. & Bergstrom D.J. (1993). Predictive models for erosion-corrosion under disturbed flow conditions, *Corrosion Science*, Vol.35, No.1-4, 627-633, ISSN 0010-938X. Poulson B. (1983). Electrochemical measurements in flowing solutions, *Corrosion Science*, Vol.23, No.4, 391-430, ISSN 0010-938X.

Poulson B. (1993). Advances in understanding hydrodynamic effects on corrosion, *Corrosion Science*, Vol.35, No.1-4, 655-665, ISSN 0010-938X.

Poulson B. (1999). Complexities in predicting erosion corrosion, *Wear*, Vol.233-235, 497-504, ISSN 0043-1648.

Sydberger T. & Lotz U. (1982). Relation Between Mass Transfer and Corrosion in a Turbulent Pipe Flow, *J. Electrochem. Soc.*, Vol.129, No.2, 276-283, ISSN 0013-4651.

Syrett B.C. (1976). Erosion-corrosion of copper-nickel alloys in seawater and other aqueous environments – a Literaturee review, *Corrosion*, Vol.32, 242-252, ISSN 0010-9312.

Wharton J.A. & Wood R.J.K. (2004). Influence of flow conditions on the corrosion of AISI 304L stainless steel, *Wear*, Vol.256, No.5, 525-536, ISSN 0043-1648.

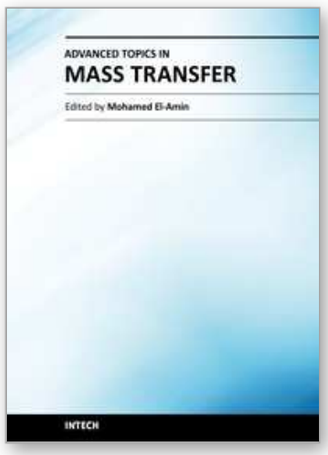

Advanced Topics in Mass Transfer

Edited by Prof. Mohamed El-Amin

ISBN 978-953-307-333-0
Hard cover, 626 pages
Publisher InTech
Published online 21, February, 2011
Published in print edition February, 2011

This book introduces a number of selected advanced topics in mass transfer phenomenon and covers its theoretical, numerical, modeling and experimental aspects. The 26 chapters of this book are divided into five parts. The first is devoted to the study of some problems of mass transfer in microchannels, turbulence, waves and plasma, while chapters regarding mass transfer with hydro-, magnetohydro- and electro- dynamics are collected in the second part. The third part deals with mass transfer in food, such as rice, cheese, fruits and vegetables, and the fourth focuses on mass transfer in some large-scale applications such as geomorphologic studies. The last part introduces several issues of combined heat and mass transfer phenomena. The book can be considered as a rich reference for researchers and engineers working in the field of mass transfer and its related topics.

InTech Europe
University Campus STeP Ri
Slavka Krautzeka 83/A
51000 Rijeka, Croatia
Phone: +385 (51) 770 447
Fax: +385 (51) 686 166
www.intechopen.com

InTech China
Unit 405, Office Block, Hotel Equatorial Shanghai
No.65, Yan An Road (West), Shanghai, 200040, China
中国上海市延安西路65号上海国际贵都大饭店办公楼405单元
Phone: +86-21-62489820
Fax: +86-21-62489821

IntechOpen